Journal of Fluids and Structures (1998) **12,** 859–882
Article No. fl980171

OSCILLATING RECTANGULAR AND OCTAGONAL PROFILES: MODELLING OF FLUID FORCES

S. Deniz†

Department of Aeronautics and Astronautics, Gas Turbine Laboratory Massachusetts Institute of Technology, Cambridge, MA 02139, U.S.A.

T. Staubli

Swiss Federal Institute of Technology, Institute of Energy Technology, Turbomachinery Laboratory, CH-8092 Zurich, Switzerland

(Received 16 January 1997 and in revised form 5 June 1998)

Fluid forces acting on rectangular and octagonal cylinders oscillating without ($\alpha = 0°$) and with ($\alpha = 10°$) a mean incidence were measured in a water channel. Experimentally determined force coefficients and phase angles were compared to calculated coefficients determined using the "unsteady airfoil theory" and the "quasi-steady theory". The results showed that calculation of the time-dependent lift force coefficient according to the quasi-steady theory can only be used at low oscillation frequencies. While the quasi-steady theory does not account for fluid inertia, the unsteady airfoil theory models the forces resulting from the cylinder acceleration and modifies the lift force with a circulation function. Accordingly, unsteady airfoil theory may be applied to a broader frequency range. One advantage of the unsteady airfoil theory is that, in addition to the lift force, the phase angle between the lift force and cylinder displacement can be calculated. By virtue of knowing this phase angle, the ranges of positive energy transfer from the fluid to the cylinder can be determined and thereby the ranges of possible self-excited cylinder oscillations. The limits to the applications of both the unsteady airfoil theory and the quasi-steady theory were examined in detail and discussed with respect to oscillation frequency and amplitude. Neither theory is capable of encompassing the instability-induced phenomena such as resonance due to vortex shedding or phase jump. For rectangular and octagonal cylinders (prisms), the influence of the oscillation amplitude was investigated in detail, through both experiments and calculation, for several excitation frequencies of interest. One important result is that for the rectangular cylinder oscillating at a constant frequency, the direction of energy transfer between the fluid and the cylinder appeared to change as a function of oscillation amplitude.

1. INTRODUCTION

For a rectangular or an octagonal cylinder oscillating transversely in a free stream (with no turbulence), the relevant parameters, are the nondimensional oscillation frequency, S_e, and the amplitude of oscillation, $\hat{\eta}$, besides the Reynolds number, Re, and the angle of attack, α. S_e is defined as $f_e D/V$, where f_e is the cylinder excitation frequency, D, the cylinder thickness, and V the free-stream velocity; $\hat{\eta}$ is defined as $\hat{y}/D$, where $\hat{y}$ is the magnitude of oscillation amplitude. In a previous paper (Deniz & Staubli 1997), we presented measurements with varying oscillation frequency, S_e, and also addressed features of the flow field as

† Current address: Praxair Inc. Technology Center, Tonawanda, NY 14151, U.S.A.

0889-9746/98/070859 + 24 $30.00

well as the formation of vortices at the leading- and trailing edge of the cylinders through flow visualization. The chosen oscillation frequency range ($S_e = 0$–$0{\cdot}6$) allowed us to investigate effects of movement-induced excitation (MIE) instability-induced excitation (IIE), and fluid inertia.

If linearity is not assumed, $\hat{\eta}$, the *amplitude of oscillation*, becomes the second important parameter to be considered, besides the oscillation frequency. The influence by the oscillation amplitude on the flow field and the forces on oscillating cylinders are less investigated than the influence by the oscillation frequency. Visualization of the flow field around a transversally oscillating circular cylinder by Griffin & Ramberg (1974) shows a well-organized vortex shedding with enhanced vortices for an oscillation amplitude $\hat{\eta} = 0{\cdot}5$, and an oscillation frequency near the natural vortex-shedding frequency. The increase in oscillation amplitude to $\hat{\eta} = 1$ at the same oscillation frequency leads to a disorganization of vortex shedding in the wake of the circular cylinder. Blevins (1990) called this phenomenon self-limitation of the vortex-induced excitation as a result of the increase in the oscillation amplitude. Williamson & Roshko (1988) describe in detail the nonlinear interactions and modification of the flow field about a circular cylinder, depending not only on the oscillation frequency but also on the oscillation amplitude.

In the second part of this paper we present fluid force and phase angle measurements on rectangular and octagonal cylinders with varying oscillation amplitude at selected oscillation frequencies without ($\alpha = 0^\circ$) and with a mean incidence ($\alpha = 10^\circ$).

A series of *mathematical models* have been proposed in an attempt to simulate and/or explain the observed experimental phenomena and results of flow-induced oscillations. Detailed overviews are provided, for example, by Dowell *et al.* (1989), Parkinson (1989), and Naudascher & Rockwell (1994). The most widely used mathematical model for predicting the MIE (Movement-Induced Excitation) of cylinders is the *quasi-steady theory* (QST) of Parkinson (Parkinson & Brooks 1961; Parkinson & Smith 1964). Quasi-steady theory is generally applied to predict the galloping oscillation of a square-section cylinder, for instance, at low-oscillation frequencies. The term *galloping* is usually applied to the large-amplitude, low-frequency oscillations of bluff profiles (Parkinson 1971). Characteristic of profiles sensitive to galloping oscillations are the negative lift-curve slopes as first described by Den Hartog (1956). On the other hand, for oscillating airfoils, Bisphlinghoff *et al.* (1957) calculated lift forces according to *unsteady airfoil theory* (UAT). Unlike quasi-steady theory, unsteady airfoil theory allows estimates of fluid inertia forces and of shed vorticity. Estimation of fluid inertia is especially important for very high oscillation frequencies, where inertia effects dominate the flow field.

Following a short survey of different mathematical models, quasi-steady theory and unsteady airfoil theory will be applied to oscillating rectangular and octagonal cylinders in the first part of this paper. By using these models, the lift force, C_L, and the phase angle, Θ, between C_L and cylinder displacement, y, are calculated. Comparison between the results of these calculations and experimental data allows to determine the range of the validity of the models investigated.

2. MATHEMATICAL MODELLING AND CALCULATION OF FLOW-INDUCED OSCILLATIONS

The oscillation (motion) of a structure in a flow is most often presented as that of a rigid cylinder in cross-flow, with discrete mass, viscous-type damping and a linear spring support for simplicity. Therefore, the equation of the motion becomes

$$m\ddot{y} + B\dot{y} + Cy = F_L(t), \tag{1}$$

where y is the cylinder displacement, m the cylinder mass, B the damping, C the stiffness, and F_L the fluid load. F_L can be written as

$$F_L(t) = \tfrac{1}{2}\rho A V^2 C_L(t), \tag{2}$$

where $C_L(t)$ is the nondimensional coefficient of the lift force, ρ the fluid density, and A the area (length $\times$ span) of the cylinder.

In this generalized form, equation (1) can be employed to describe the response of cylinders to any type of fluid-dynamic excitation. Equation (1) can be solved, if information is available on $C_L(t)$. $C_L(t)$ can be modelled as a nonlinear function of $\mathrm{d}y/\mathrm{d}t$ (the quasi-steady theory of galloping), or is regarded as being itself governed by an additional coupled nonlinear differential equation [the fluid oscillator theory of Hartlen & Currie (1970) for vortex-induced oscillations]. Furthermore, for the calculation of $C_L(t)$, flow field models can also be used [meaning the solution of the time-dependent Navier–Stokes equations (Franke 1991; Tamura & Kuwahara 1992) or using a linearized potential flow theory (Kármán & Sears 1938) or a discrete-vortex model (Sarpkaya 1989)].

In this paper two different models will be used, to be described in Sections 2.1 and 2.2.

2.1. The Quasi-Steady Theory

At low oscillation frequencies ($S_e \to 0$) *quasi-steady* conditions should hold between lift force and $\dot{y}$:

$$C_L = f\left(\frac{\dot{y}}{V}\right) \quad \text{with } \alpha = \tan^{-1}\left(\frac{\dot{y}}{V}\right). \tag{3}$$

Quasi-steady theory is based on the mean force curves measured at a stationary cylinder. It should be noted that, for galloping calculations, the transverse fluid force, C_y, is used according to quasi-steady theory instead of the lift force, C_L, because the quasi-steady instability criterion according to Den Hartog (1956) is defined by

$$\frac{\mathrm{d}C_y}{\mathrm{d}\alpha} = \frac{\mathrm{d}C_L}{\mathrm{d}\alpha} + C_D < 0, \tag{4}$$

where C_L and C_D are the lift and drag coefficient, respectively, and C_y is the transverse fluid force coefficient ($C_y = C_L$ for $\alpha = 0^\circ$).

Quasi-steady theory assumes that at any instant during an oscillation cycle the cylinder experiences the same force, C_y, as it would if held stationary at an angle of attack, α, and subject to a relative flow velocity, V_{rel}. The relative flow velocity, V_{rel}, arising from the transverse cylinder velocity, $\mathrm{d}y/\mathrm{d}t$, can be expressed from the velocity triangle as follows:

$$V_{rel} = \sqrt{V^2 + (\mathrm{d}y/\mathrm{d}t)^2}. \tag{5}$$

Consequently, according to quasi-steady theory, the instantaneous excitation force acting on the oscillating cylinder is assumed to be equal to the stationary force evaluated at the instantaneous angle of attack α, provided that the cylinder velocity $\mathrm{d}y/\mathrm{d}t$ is small compared to the incoming flow velocity V (in other words, provided S_e is sufficiently small).

The required input for the quasi-steady theory is given by the measurement of the force coefficient, C_y, as a function of angle of attack, α, on the stationary rectangular and octagonal cylinders (Figure 1). The experimental variation of C_y versus α can be represented by an odd power polynomial,

$$C_y(\alpha) = A_1(\alpha) - A_3(\alpha)^3 + A_5(\alpha)^5 - A_7(\alpha)^7; \tag{6}$$

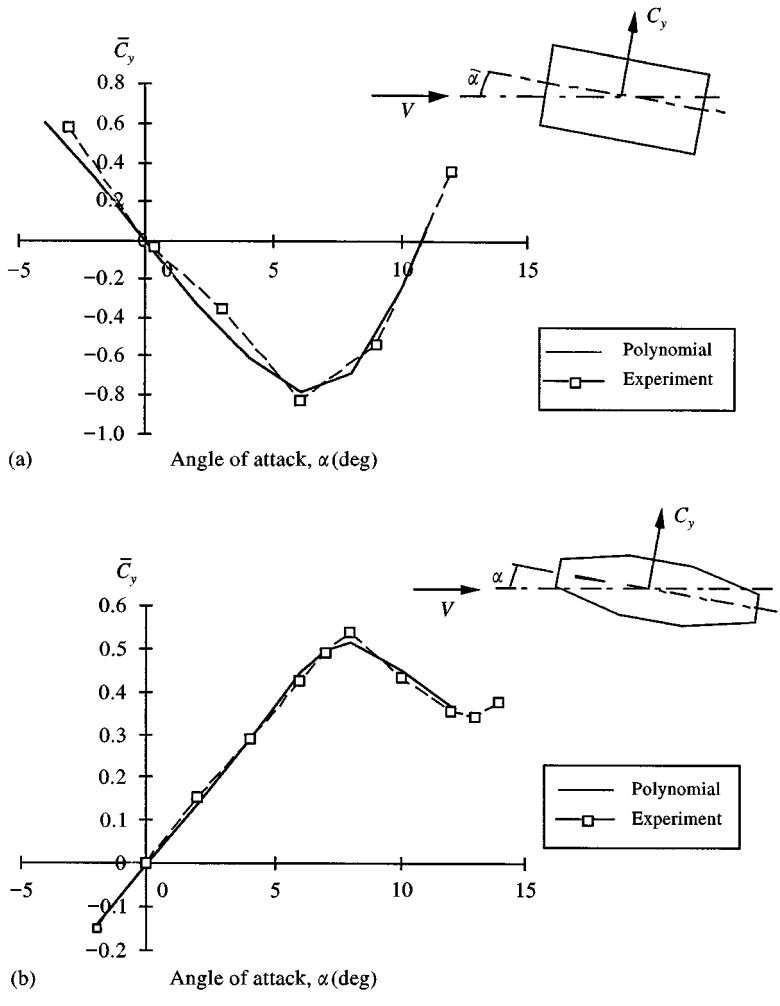

Figure 1. Transverse fluid force curves of the nonoscillating (a) rectangular and (b) octagonal cylinder with polynomial approximations for $\mathrm{Re} = 10^5$; $\hat{\eta} = 0$, $S_e = 0$.

with $\alpha = \arctan[(\mathrm{d}y/\mathrm{d}t)/V]$, from equation (6) it follows that

$$C_y\left(\frac{\dot{y}}{V}\right) = A_1\left(\frac{\dot{y}}{V}\right) - A_3\left(\frac{\dot{y}}{V}\right)^3 + A_5\left(\frac{\dot{y}}{V}\right)^5 + A_7\left(\frac{\dot{y}}{V}\right)^7. \tag{7}$$

2.2. The Unsteady Airfoil Theory

In 1935, Theodorsen presented a potential-flow theory defining the lift and moment experienced by a flat plate, undergoing a small amplitude oscillation (via linearization) in a uniform incompressible flow. Later, for an airfoil oscillating transversely in incompressible flow, Bisplinghoff *et al.* (1957) showed that the lift force per unit span induced by oscillation motion is given by

$$F_L = F_{L1} + F_{L2} = -\lambda\rho\pi\left(\frac{L}{2}\right)^2 \ddot{y} - \rho V \frac{L}{2}\frac{\partial C_L}{\partial \alpha} C(k)\,\dot{y}, \tag{8}$$

where λ is the added mass or flow inertia coefficient, V the incoming flow velocity, $\partial C_L/\partial\alpha$ the lift-curve slope ($\partial C_L/\partial\alpha = 2\pi$ theoretically for a diminishingly thin boundary layer and wake), k the reduced circular frequency (that is equal to $2\pi S_e$), and $C(k) = F(k) + \mathrm{i}G(k)$ is the complex Theodorsen's circulation function.

For the idealized flow theory, the lift force depends on the circulation of the fluid around an airfoil which in turn is determined by satisfying the Kutta condition at the trailing edge. In the case of unsteady motion, however, the airfoil motion changes the circulation around it and the lift is no longer a simple function of the circulation. The change in circulation is accompanied by vortex shedding from the trailing edge. In addition, the nonuniform motion or acceleration of the fluid particles around the airfoil gives rise to fluid dynamic inertia forces (Brar *et al.* 1996).

F and G are the real and imaginary portions of $C(k)$ and they are functions of the reduced frequency as shown in Figure 2. $C(k)$ may be expressed in terms of modified Hankel functions of the first and second kind of order zero and one:

$$C(k) = \frac{\mathrm{H}_1^{(2)}(k)}{\mathrm{H}_1^{(2)}(k) + \mathrm{i}\mathrm{H}_0^{(2)}(k)} \quad \text{with } k = \omega_e D/V = 2\pi S_e. \tag{9}$$

Substituting $C(k) = F(k) + \mathrm{i}G(k)$ into equation (9) leads to

$$F_L = -\lambda\rho\pi\left(\frac{L}{2}\right)^2 \ddot{y} - \rho V \frac{L}{2}\frac{\partial C_L}{\partial\alpha} F(k)\dot{y} + \rho V \frac{L}{2}\frac{\partial C_L}{\partial\alpha} G(k)\omega y. \tag{10}$$

With the fluid dynamic (or added) mass, A', fluid-dynamic damping, B', and fluid-dynamic rigidity, C', equation (10) has the form of body oscillators [cf. equation (1)]:

$$F_L = -A'\ddot{y} - B'\dot{y} - C'y. \tag{11}$$

The decomposition of the total lift into components relies on linear assumptions allowing the superposition. The first component in equation (8), F_{L1}, is the noncirculatory term (owing to its independence from V) which is recognized as the fluid inertia force. The second term, F_{L2}, represents the effect of flow circulation about the body. For an airfoil oscillating transversely to a free stream, the lift force acting on the airfoil, hence the circulation around it, varies continuously. In order to satisfy Kelvin's circulation theory ($\mathrm{D}\Gamma/\mathrm{D}t = 0$), vorticity must be shed by the airfoil and the shed vorticity, Γ, remains conserved. The vorticity shed can affect the flow around the airfoil, and thus the lift force acting on it in terms of magnitude and phase (Luo & Bearman 1990). The Theodorsen function is a complex function and, therefore, a phase angle Θ between lift and displacement of the body results.

It should be noted that the unsteady airfoil theory, which will be applied to oscillating rectangular and octagonal cylinders, was originally derived to describe fluid forces on thin airfoils oscillating with small amplitudes. However, it also allows to make estimates of inertia and shed vorticity for bluff bodies as demonstrated by Luo & Bearman (1990), Matsumoto *et al.* (1995), and Matsumoto (1971) for the prediction of the lift force and phase angle on a transversely oscillating square-section cylinder. The Theodorsen function and unsteady airfoil theory are widely used for stability analysis and estimation of the lift and the moment experienced by profiles undergoing flutter oscillations. Two typical areas, where unsteady airfoil theory is applied, are flutter oscillations of airfoils and turbo-machinery blades, as well as bridge decks. Since most bridge-deck profiles are relatively bluff, having flow separation around them, unsteady airfoil theory appears not to be an appropriate tool for the bridge-flutter problem. On the other hand, unsteady airfoil theory

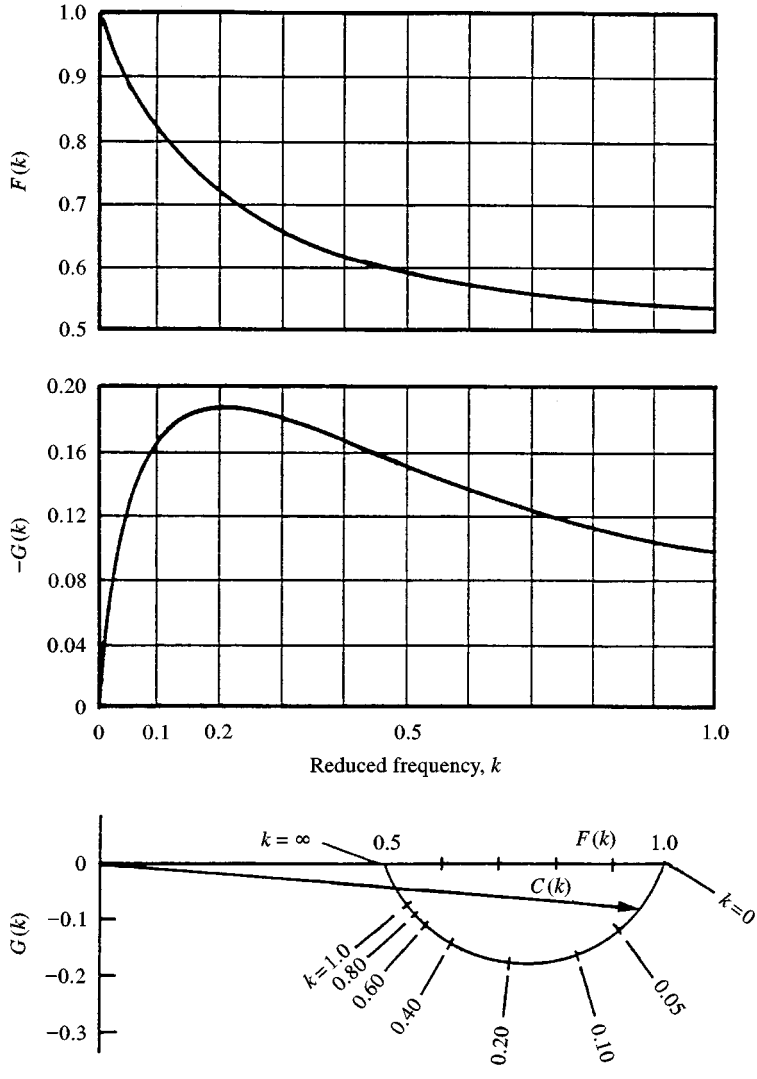

Figure 2. Theodorsen function, $C(k) = F(k) + iG(k)$.

is used to obtain flutter derivatives and force coefficient gradients of bridge-deck profiles, successful and failed examples for which can be found in the open literature [e.g. Scanlan & Tomko (1971), Scanlan *et al.* (1974), and a general overview incorporating several examples by Försching (1974)].

In the following analysis, we only examine the component of the lift force F_{Le} at the excitation frequency S_e. Substituting the harmonic motion of the body $y = \hat{y}\cos\omega t$ and its derivatives into equation (10), we obtain

$$F_{Le} = F_{Le1} + F_{Le2} = \left[\lambda\rho\pi\left(\frac{L}{2}\right)^2 \omega + \rho V \frac{L}{2}\frac{\partial C_L}{\partial\alpha} G(k)\right](\hat{y}\omega\cos\omega t) + \left[\rho V \frac{L}{2}\frac{\partial C_L}{\partial\alpha} F(k)\right]$$

$$\times(\hat{y}\omega\sin\omega t). \tag{12}$$

F_{Le1} and F_{Le2} can be written in a nondimensional form as

$$C_{Le1} = \frac{F_{Le1}}{-\rho\pi\left(\frac{L}{2}\right)^2 \ddot{y}} = \frac{[\lambda\rho\pi(L/2)^2\omega + \rho V(L/2)(\partial C_L/\partial\alpha)\,G(k)]\,(\hat{y}\omega\cos\omega t)}{-\rho\pi(L/2)^2(-\hat{y}\omega^2\cos\omega t)}, \tag{13}$$

$$C_{Le1} = \lambda + \frac{\partial C_L}{\partial\alpha}\,G(k)\frac{1}{2\pi k}, \tag{14}$$

$$C_{Le2} = \frac{F_{Le2}}{\frac{1}{2}\rho L V^2} = \frac{\rho V(L/2)(\partial C_L/\partial\alpha)\,F(k)\hat{y}\omega\sin\omega t}{\frac{1}{2}\rho L V^2}, \tag{15}$$

with

$$\tan\hat{\alpha} = \frac{\hat{\dot{y}}}{V} = \frac{2\pi f_e\hat{y}}{V} = 2\pi\frac{\hat{y}}{D}\frac{f_e D}{V} = 2\pi\hat{\eta}S_e, \tag{16}$$

$$C_{Le2} = \frac{\partial C_L}{\partial\alpha}\,F(k)\tan\hat{\alpha}\sin\omega t, \tag{17}$$

$$C_{Le2} = \hat{C}_{Le2}\sin\omega t. \tag{18}$$

Equation (8) can also be written in a nondimensional form:

$$C_{Le} = \frac{F_{Le}}{\frac{1}{2}\rho L V^2} = \frac{F_{Le1} + F_{Le2}}{\frac{1}{2}\rho L V^2} = \frac{-C_{Le1}\rho\pi\left(\frac{L}{2}\right)^2\ddot{y} + C_{Le2}\rho L\frac{V^2}{2}}{\frac{1}{2}\rho L V^2}, \tag{19}$$

$$C_{Le} = -C_{Le1}\pi\left(\frac{L}{2}\right)\frac{1}{V^2}\ddot{y} + C_{Le2}. \tag{20}$$

Substituting C_{Le2} from equation (17) into equation (20) and using the fact that $L = 2D$ for a rectangular cylinder, equation (20) becomes

$$C_{Le} = C_{Le1}2\pi^2\tan\hat{\alpha}S_e\cos\omega t + \frac{\partial C_L}{\partial\alpha}\,F(k)\tan\hat{\alpha}\sin\omega t. \tag{21}$$

We can also use a harmonic assumption for the lift component at the excitation frequency, C_{Le}:

$$C_{Le} = \hat{C}_{Le}\cos(\omega t + \Theta), \tag{22}$$

$$C_{Le} = \hat{C}_{Le}\cos\Theta\cos\omega t - \hat{C}_{Le}\sin\Theta\sin\omega t. \tag{23}$$

From equations (21) and (23), we have

$$\hat{C}_{Le}\cos\Theta = C_{Le1}2\pi^2\tan\hat{\alpha}S_e,$$

$$\hat{C}_{Le}\sin\Theta = -\frac{\partial C_L}{\partial\alpha}\,F(k)\tan\hat{\alpha}. \tag{24}$$

The magnitude of the lift component at the excitation frequency becomes

$$\hat{C}_{Le} = \sqrt{(C_{Le1}2\pi^2\tan\hat{\alpha}\mathrm{S})^2 + \left(\frac{\partial \mathrm{C}_L}{\partial\alpha}F(k)\tan\hat{\alpha}\right)^2}, \tag{25}$$

and the phase shift between the lift component and the body motion

$$\Theta = \tan^{-1}\left[\frac{-(\partial C_L/\partial\alpha)\,F(k)}{2C_{Le1}\pi^2 S_e}\right], \tag{26}$$

with

$$C_{Le1} = \lambda + \frac{1}{2\pi k}\frac{\partial C_L}{\partial\alpha}\,G(k). \tag{27}$$

A few observations can be made from equations (25)–(27). First, in equation (26) the sign of the slope of the lift curve, $\partial C_L/\partial\alpha$, determines the range of phase angle and thus the direction of energy transfer between the fluid and the cylinder. Second, the calculation of the magnitude of the lift force, $\hat{C}_{Le}$, in equation (25) takes both the oscillation frequency (with the terms S_e and $\tan\hat{\alpha}$) and the oscillation amplitude (with the term $\tan\hat{\alpha}$) into account. On the other hand, the calculation of the phase angle according to unsteady airfoil theory in equation (26) is independent of the oscillation amplitude. Finally, the noncirculatory part of the lift force, C_{Le1}, in equation (27) contains the flow inertia coefficient, λ, and an additional term $(1/2\pi k)\,(\partial C_L/\partial\alpha)\,G(k)$. This additional term modifies the potential flow inertia coefficient and is, therefore, called the "added inertia coefficient" by Luo & Bearman (1990).

The nondimensional added mass (or flow inertia) coefficient, λ, is defined by the added mass formulation, which gives the relationship between lift force and cylinder acceleration, $\ddot{y}$, i.e.

$$F_{\mathrm{Lad}} = -\lambda\rho\pi\left(\frac{L}{2}\right)^2\ddot{y}; \tag{28}$$

λ can be determined from the potential flow theory and/or experiment at zero flow conditions (oscillation in a still fluid). The added mass coefficients for the profiles investigated were calculated by Groh (1992). They are $\lambda_R = 1{\cdot}36$ for the rectangular cylinder, and $\lambda_O = 1{\cdot}103$ for the octagonal cylinder. The added mass calculation is also useful to check the validity of mathematical models for $S_e \to \infty$.

3. EXPERIMENTS

The experimental facility is described in Deniz & Staubli (1997); further details can be found in Deniz (1993) and Staubli (1983).

For the investigations with oscillating cylinders, the data are presented as a function of the nondimensional oscillation frequency, S_e, and the relative oscillation amplitude, $\hat{\eta}$. During the experiments the nondimensional oscillation frequency was varied for the octagonal cylinder up to $S_e = 0{\cdot}55$ and for the rectangular cylinder up to $S_e = 0{\cdot}26$, while the relative amplitude of oscillation up to $\hat{\eta} \approx 2$, depending on the oscillation frequency. The maximum oscillation amplitude investigated becomes smaller with increasing oscillation frequency, because of the limited capacity of the experimental facility. Measured values of externally excited lift coefficient, $\hat{C}_{Le}$, will be normalized with the relative oscillation amplitude, $\hat{\eta}$, and plotted as $\hat{C}_{Le}/\hat{\eta}$ in Figures 3–6.

4. RESULTS

4.1. Validation of the Mathematical Models

For the rectangular and octagonal cylinders investigated, Figure 1(a,b) shows both the nondimensionalized forces acting on the stationary cylinders for varying angle of attack, α,

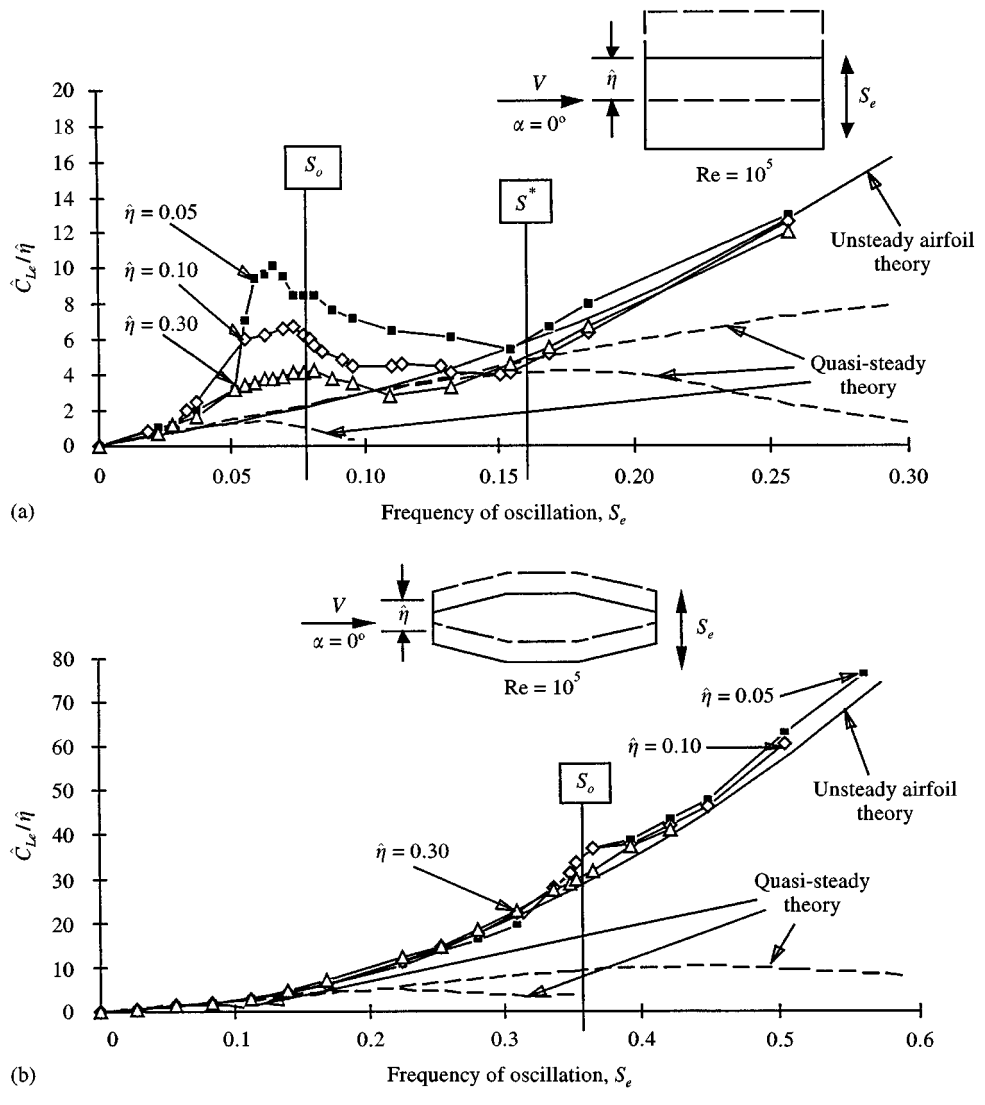

Figure 3. Normalized lift coefficient $\hat{C}_{Le}/\hat{\eta}$ of the (a) rectangular cylinder and (b) octagonal cylinder for different oscillation amplitudes, $\hat{\eta}$, as a function of the dimensionless oscillation frequency, S_e, for $\mathrm{Re} = 10^5$ and $\alpha = 0°$; comparison of experiment with the quasi-steady theory and the unsteady airfoil theory.

and also the polynomial approximations of these experimental C_y curves. The change in sign of $\partial C_y/\partial\alpha$ for the rectangular cylinder at $\alpha \approx 6°$ is caused by the reattachment of flow on one side of the cylinder, whereas for the octagonal cylinder at $\alpha \approx 8°$ the change is caused by the upstream shifting of flow separation from the trailing edge on one side of the profile with increasing angle of attack [as discussed in Deniz & Staubli (1997)].

The polynomial coefficients A_i, [equation (6)] which gave best fit to the experimental data for incidence $-12° < \alpha < 12°$ are displayed in Table 1. The slopes $\partial C_y/\partial\alpha$ at $\alpha = 0°$ and $\alpha = 10°$, extracted from the data of Figure 1, are also shown in the same table.

In Figures 3–6, the experimental data which are taken for varying excitation frequency, S_e, at three different oscillation amplitudes, $\hat{\eta}$, are compared to the results of the calculations employing both the quasi-steady and the unsteady airfoil theory. (In Figures 3–6, the top

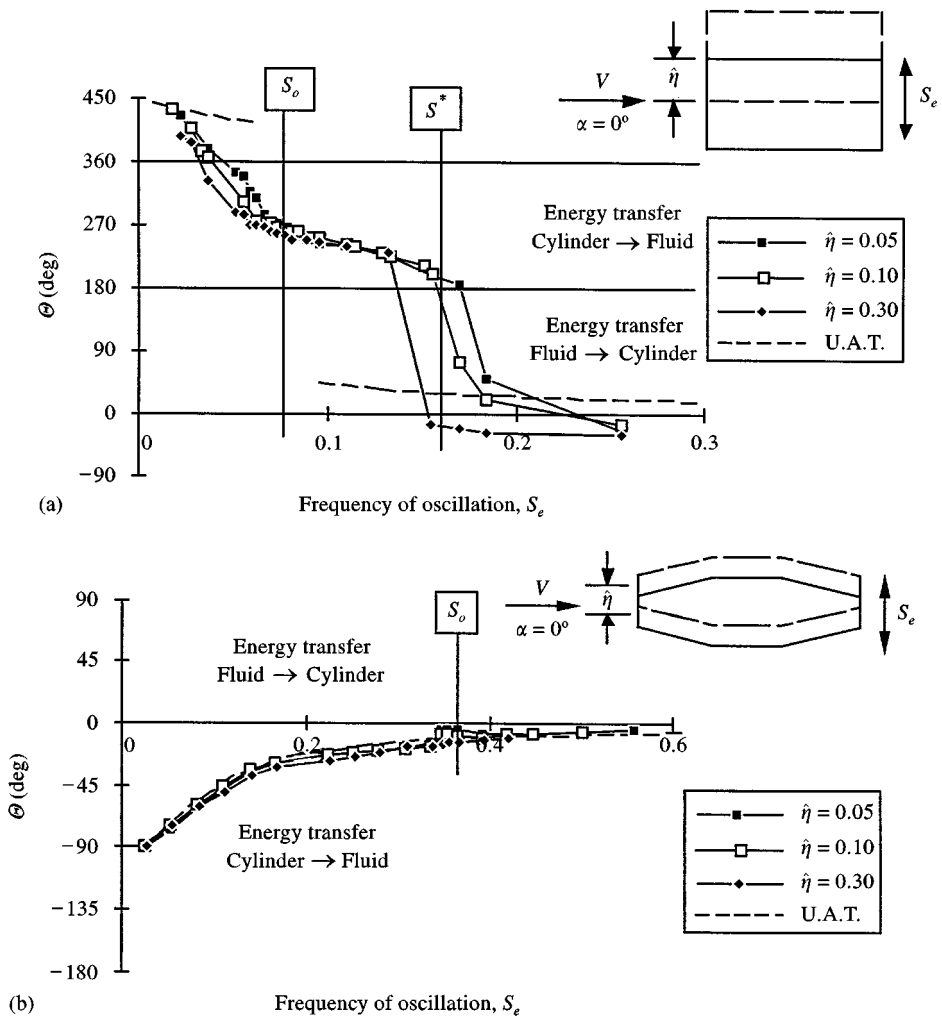

Figure 4. Phase angle Θ of the (a) rectangular cylinder and (b) octagonal cylinder for different oscillation amplitudes $\hat{\eta}$ as a function of the dimensionless oscillation frequency S_e, for Re = 10^5 and $\alpha = 0°$; comparison of experiment with the unsteady airfoil theory (UAT).

diagram, (a), shows results for the rectangular cylinder; the bottom diagram, (b), for the octagonal cylinder.) The nondimensional instability frequencies, the frequency of wake vortex formation (Kármán vortex-shedding frequency) S_o, and frequency of impinging vortices S^*, are marked in Figures 3–6. S_o and S^* are obtained on stationary cylinders.

In Figure 3 the normalized lift coefficient $\hat{C}_{Le}/\hat{\eta}$ and in Figure 4 the phase angle Θ between lift and displacement are plotted for oscillations with zero mean incidence ($\alpha = 0°$). Since the unsteady airfoil theory assumes a linear relationship between the lift force and the amplitude of oscillation, curves collapse into one single curve for different amplitudes of oscillation, $\hat{\eta}$. The quasi-steady theory distinguishes three different curves with respect to the three different amplitudes of oscillation. However, at low oscillation frequencies (where the quasi-steady theory is only valid), the differences between three curves are negligibly small.

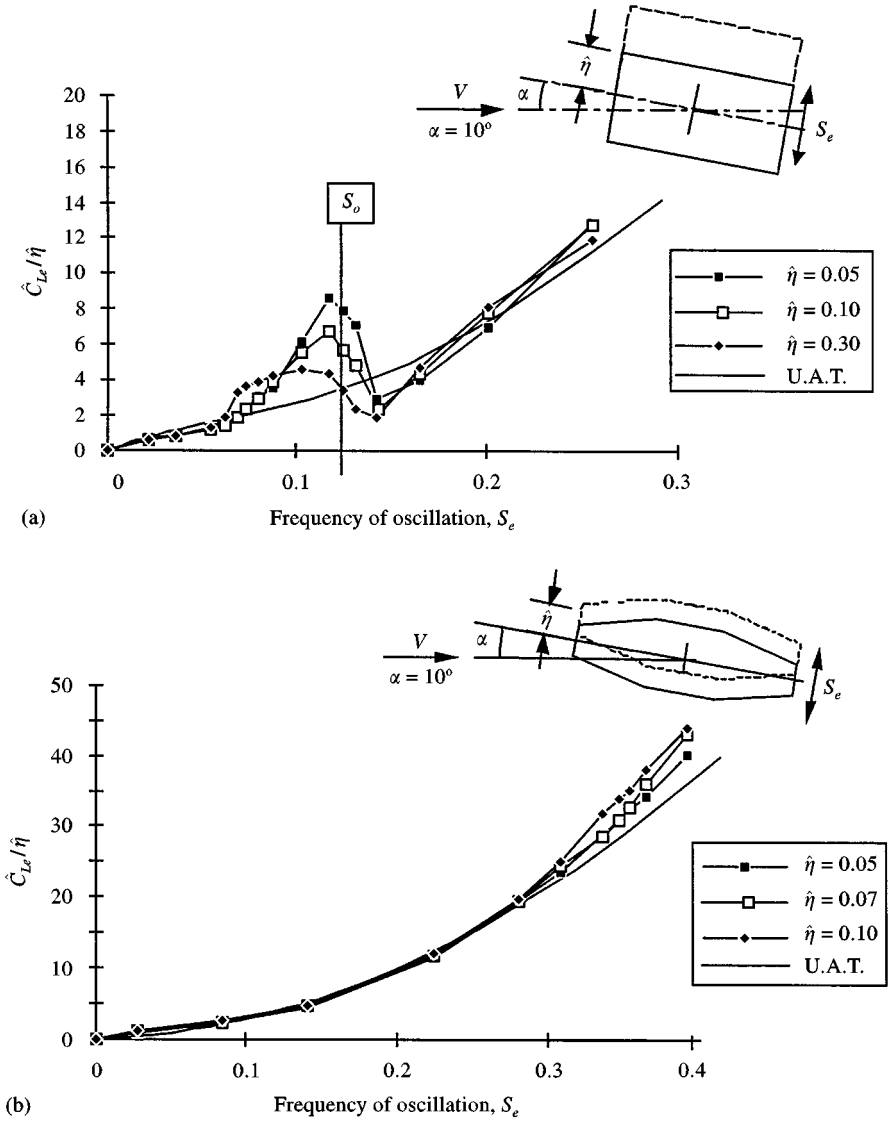

Figure 5. Normalized lift coefficient $\hat{C}_{Le}/\hat{\eta}$ of the (a) rectangular cylinder and (b) octagonal cylinder for different oscillation amplitudes, $\hat{\eta}$, as a function of oscillation frequency S_e, for $\mathrm{Re} = 10^5$ and $\alpha = 10°$; comparison of experiment with the unsteady airfoil theory (UAT).

As far as the lift coefficients are concerned, the unsteady airfoil theory and the quasi-steady theory agree well with each other for low oscillation frequencies (for the rectangular cylinder $S_e < 0{\cdot}06$; for the octagonal cylinder $S_e < 0{\cdot}08$). The quasi-steady theory was developed to predict galloping oscillations which occur at low frequencies ($S_e < 0{\cdot}05$). In this low oscillation-frequency range, agreement between calculations and measurements is good for both cylinders. For the rectangular cylinder deviation between calculation and measurements starts at lower oscillation frequencies ($S_e \approx 0{\cdot}04$), because the interaction between Kármán vortex shedding in the wake and cylinder oscillation begins to dominate the force coefficient. It should be noted that, for the rectangular cylinder, the Kármán vortex

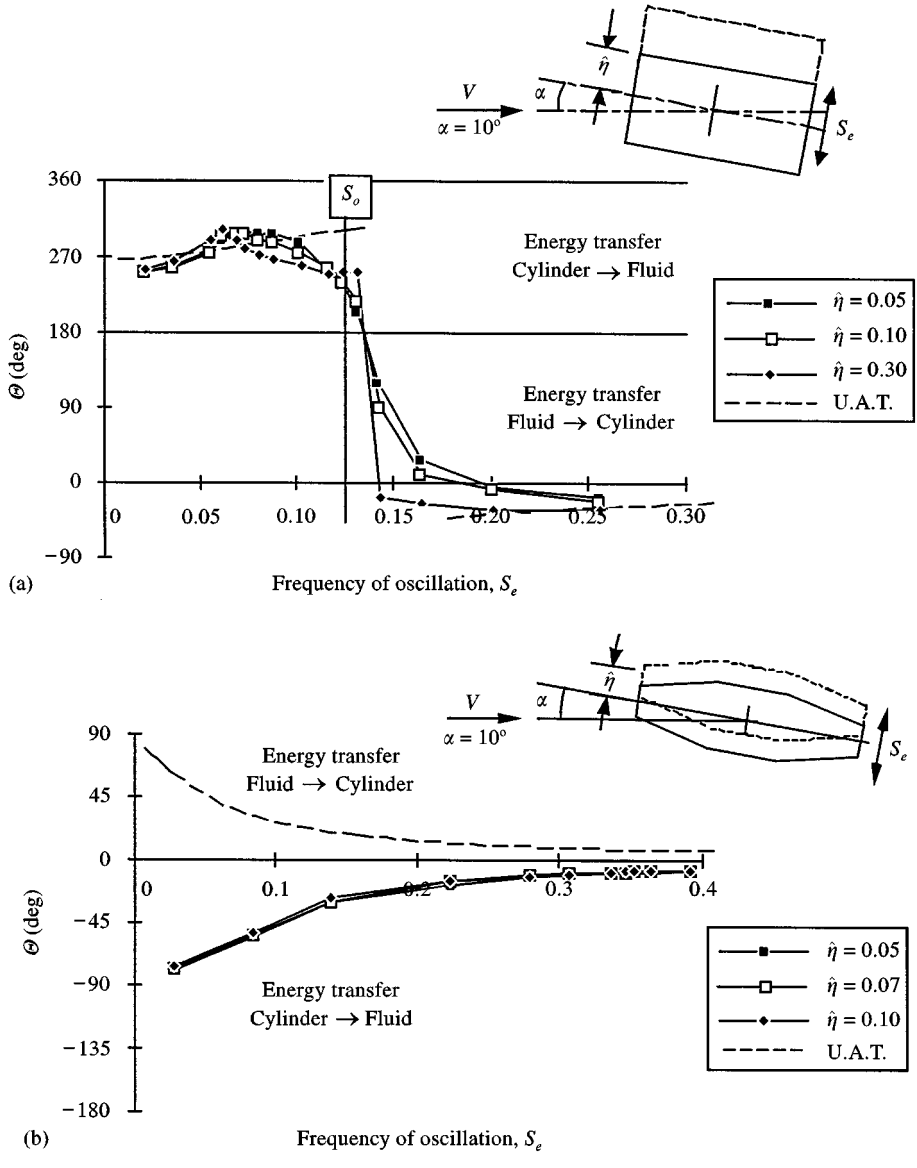

Figure 6. Phase angle Θ of the (a) rectangular cylinder and (b) octagonal cylinder for different oscillation amplitudes $\hat{\eta}$ as a function of oscillation frequency S_e for Re $= 10^5$ and $\alpha = 10°$; comparison of experiment with the unsteady airfoil theory (UAT).

TABLE 1

The polynomial coefficients A_i and values of $\partial C_y/\partial\alpha$

Profile	A_1	A_2	A_3	A_4	$\partial C_y/\partial\alpha$ ($\alpha = 0°$)	$\partial C_y/\partial\alpha$ ($\alpha = 10°$)
Rectangular cylinder	− 5·75	− 42·4	11 000	187 000	− 4·85	6·32
Octagonal cylinder	3·85	− 120·7	− 8760	− 112 255	4·62	− 3·34

shedding frequency is $S_o = 0{\cdot}078$, which is smaller than that for other elongated profiles (see for comparison Deniz & Staubli 1997). Therefore, resonance with Kármán vortex-shedding frequency affects lift coefficients at lower oscillation frequencies, where galloping oscillations may usually occur and the quasi-steady theory is applicable.

The upper bound of oscillation frequency, at which the quasi-steady theory is valid, is not theoretically obtainable, but as suggested both in Figure 3(a) and in experiments by Nakamura & Mizota (1975), the upper bound is associated with vortex shedding. When the vortex resonance frequency is approached, interaction between galloping and vortex excitation takes place. This subject was investigated by Bearman *et al.* (1987) for an oscillating square-section cylinder. Vortex excitation occurs within a certain range of oscillation frequency, at which the instability frequency such as Kármán vortex-shedding frequency coincides with the oscillation frequency of the cylinder. In the case of the rectangular cylinder, a broad frequency range exists, where vortex interaction occurs and instability-induced phenomena, such as wake vortex shedding and impinging vortices, dominate the flow field and the fluid forces. Neither theory is valid in this frequency range. However, for high oscillation frequencies ($S_e > 0{\cdot}25$), where the fluid inertia forces dominate, there is decent agreement between the results obtained by the unsteady airfoil theory and measurements [Figure 3(a)]. Compared to the rectangular cylinder, the lift amplification due to vortex resonance is small for the octagonal cylinder and also occurs in a very narrow frequency range. Therefore, the prediction of lift coefficients of the octagonal cylinder with the unsteady airfoil theory agrees with the experimental data in a broad frequency range [Figure 3(b)].

The phase angle Θ determines the direction of energy transfer between the fluid and the oscillating cylinder. Accordingly, an elastically mounted cylinder would undergo self-excited oscillations for the ranges of oscillation frequencies and amplitudes where energy transfer occurs from the fluid to the cylinder. These ranges are explicitly shown in all phase graphs. According to the quasi-steady theory, the phase angle Θ is $\pi/2 = 90^\circ$ and remains constant (corresponding to $2\pi + \pi/2 = 450^\circ$ for the figure of the rectangular cylinder) in which C_{Le} is assumed to be in phase with $\mathrm{d}y/\mathrm{d}t$ for all flow velocities. The measurements show a progressive approach to the quasi-steady phase angle condition for very low oscillation frequencies (Figure 4). For oscillations without a mean incidence ($\alpha = 0^\circ$), calculations of phase angle according to the unsteady airfoil theory always show energy transfer from the fluid to the cylinder for the rectangular cylinder, while in the opposite direction for the octagonal cylinder. This is expected, because in the vicinity of $\alpha = 0^\circ$, for the rectangular cylinder $\partial C_y/\partial\alpha$ is negative, and for the octagonal cylinder $\partial C_y/\partial\alpha$ is positive. The experimentally determined phase curve of the rectangular cylinder shows steep gradients and changes, such as a phase jump due to instability-induced phenomena. Such phase jumps are inherent to vortex interactions, observed in many different types of cylinders, but obviously these jumps cannot be predicted by unsteady airfoil theory. According to Figure 4(a), unsteady airfoil theory can only estimate the phase angle for low oscillation frequencies, where movement-induced galloping oscillations occur for the rectangular cylinder at $\alpha = 0^\circ$. On the other hand, phase-angle curves of the octagonal cylinder do not show big changes with varying oscillation frequency and amplitude due to the instability-induced phenomena, as seen in Figure 4(b). Therefore, unsteady airfoil theory predicts well the experimental data for phase angle of the octagonal cylinder at $\alpha = 0^\circ$.

For the case of oscillations with a mean incidence of $\alpha = 10^\circ$, the predictions according to unsteady airfoil theory are shown in Figures 5 and 6, together with the experimental results. In Figure 5(a), for the rectangular cylinder, unsteady airfoil theory is only capable of predicting the trend of the experimentally measured lift curve at low and high frequencies.

In the frequency range where the frequency of oscillation is close to the cylinder vortex-shedding frequency S_o, unsteady airfoil theory cannot be used. For the $\hat{C}_{Le}/\hat{\eta}$ curve of the octagonal cylinder in Figure 4(b), agreement between the experimental results and the unsteady airfoil theory is better, because no effects of instability-induced phenomena on the lift force occur for the octagonal cylinder.

For the rectangular cylinder, unsteady airfoil theory predicts the trend of the curves of the phase angle for $\alpha = 10^\circ$ [Figure 6(a)]. Again, the phase jump is not predictable by this theory. Except for the range of the phase jump, unsteady airfoil theory estimates the direction of the energy transfer correctly for the rectangular cylinder at $\alpha = 10^\circ$. Unfortunately, this is not true for the phase angle prediction in the case of the octagonal cylinder in Figure 6(b) for $\alpha = 10^\circ$. The reason for this difference is that unsteady airfoil theory requires the slope of the C_L-curve at $\alpha = 10^\circ$ for prediction of the phase angle—see equation (26). $\partial C_L/\partial\alpha$ is slightly negative for $\alpha = 10^\circ$ and therefore the prediction of phase angle, which does not agree with the experimental data, indicates an energy transfer from the fluid to the cylinder. The case of the octagonal cylinder for $\alpha = 10^\circ$ is a unique case, where Den Hartog's instability criterion is not satisfied. According to Den Hartog's instability criterion ($\partial C_y/\partial\alpha < 0$), galloping oscillations may occur for the octagonal cylinder at $\alpha = 10^\circ$, due to the slightly negative slope of the C_y versus α curve in this range. Phase angle measurements of the octagonal cylinder in Figure 6(b) do not indicate any region where energy transfer occurs from the fluid to the cylinder, and therefore no galloping oscillations occur for $\alpha = 10^\circ$. In several published investigations, Novak showed that quasi-steady theory is in good agreement with the experimental results for galloping oscillations of bluff cylinders. Moreover, Novak tested Den Hartog's instability criterion for different types of cylinders. In many practical cases, examination of Den Hartog's instability criterion alone suffices to assess proclivity of a structure to galloping, even though the phenomena are, in fact, strongly nonlinear. Novak (1972) identified various forms of $C_y(\alpha)$ curves and the trends of the corresponding galloping response amplitudes, each as a function of the reduced velocity parameter $V_r = 1/\mathrm{S}$. There exist situations (e.g., for a rectangular cylinder with the length ratio of $L/D = 0{\cdot}5$), wherein galloping oscillations take place, even though Den Hartog's instability criterion ($\partial C_y/\partial\alpha < 0$) is not satisfied.

Lift force predictions according to the unsteady airfoil theory require the calculation of the added mass or flow inertia coefficient, λ. Using the added mass coefficients given in Section 2, forces, which were calculated for the cases with zero incidence ($\alpha = 0^\circ$) and for a mean incidence of $\alpha = 10^\circ$, are compared with the forces acting on the cylinder in a still fluid (no flow, $V = 0$). Calculated and measured lift forces due to added mass agree well, except for very high oscillation frequencies. For oscillations in a still fluid, a phase angle of 0° is expected, as experimentally confirmed at the low oscillation frequencies, whereas for the high frequencies, measured phase angles deviate a few degrees from 0° and become negative (Deniz 1993).

4.2. Influence of the Oscillation Amplitude

The effects of nonlinearity in response to the amplitude of oscillation are the greatest in the range of vortex synchronization frequencies; see Figures 3–6. Especially the oscillation frequency, where a phase jump occurs, the width of vortex resonance range and the maximum lift coefficients in this range depend on the amplitude of oscillation. The maximum value of the oscillation amplitude investigated has been until now $\hat{\eta} = 0{\cdot}30$. In practice, particularly, in the case of galloping oscillations, the amplitude of the oscillation can be higher. For this reason, selected frequencies were investigated with higher amplitudes of oscillation, as shown in Figures 7–9 for the rectangular and octagonal cylinders, and both

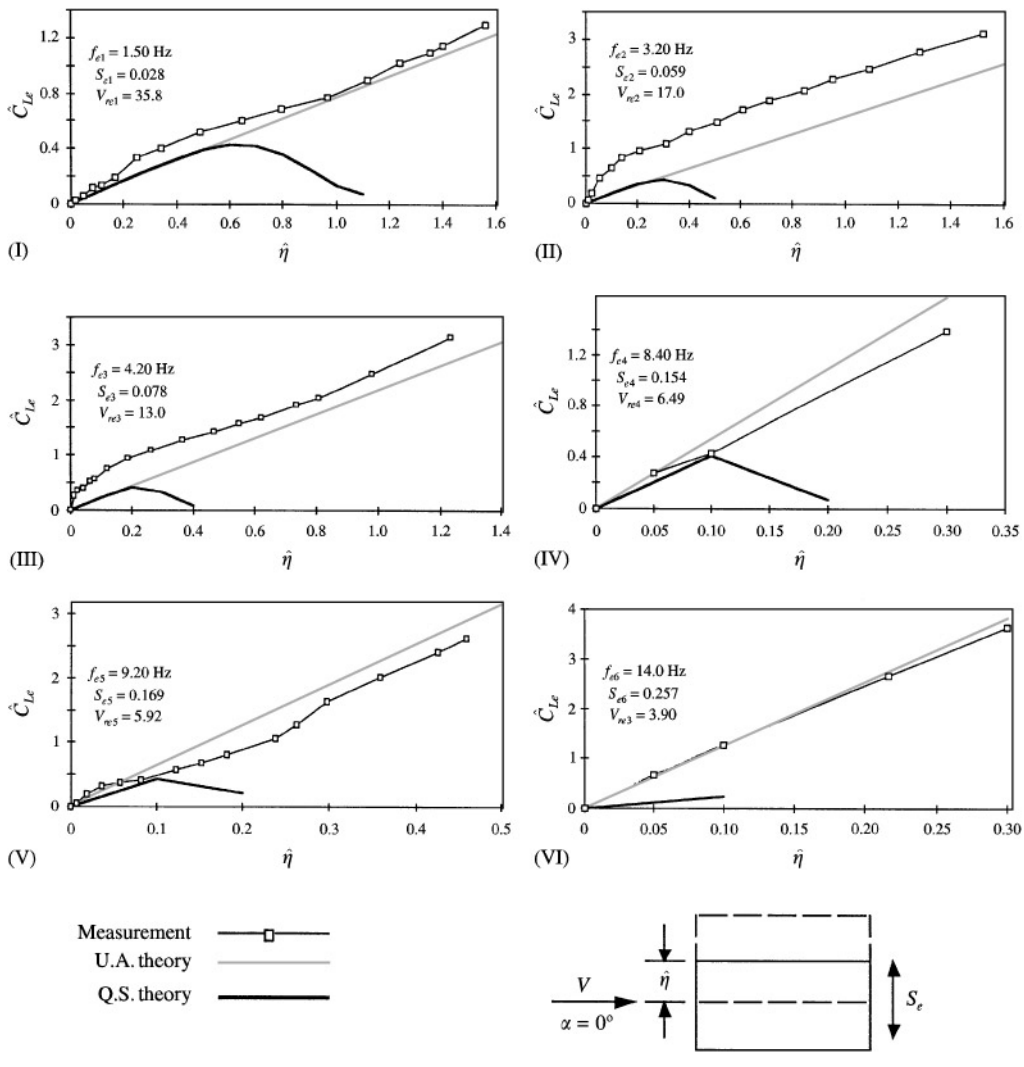

Figure 7(a) Lift coefficient $\hat{C}_{Le}$ of the rectangular cylinder for different oscillation frequencies, S_e (I–VI) as a function of the dimensionless oscillation amplitude $\hat{\eta}$, for Re $= 10^5$ and $\alpha = 0°$; comparison of experiment with the quasi-steady (QS) theory and the unsteady airfoil (UA) theory.

without ($\alpha = 0°$) and with ($\alpha = 10°$) a mean incidence. In Figures 7–9 data are shown for six constant excitation frequencies S_e, although more excitation frequencies were investigated in the course of this investigation (Deniz 1993). The six excitation frequencies presented in Figures 7–9 were chosen such that one low frequency is in the galloping range, four frequencies are near the frequency of Kármán vortex shedding, S_o, and near the frequency of impinging vortices, S^*, and one very high frequency is in the range of added mass.

For $\alpha = 0°$, both $\hat{C}_{Le}$ and Θ, predicted by the unsteady airfoil theory and the quasi-steady theory, are also included in Figure 7 (for the rectangular cylinder) and Figure 8 (for the octagonal cylinder). In Figures 7–9 the different excitation frequencies investigated are numbered with Roman numerals (I–VI), and the values for the relevant parameters such as the nondimensional excitation frequency, S_e, and reduced velocity $V_{re} = 1/S_e$ are given.

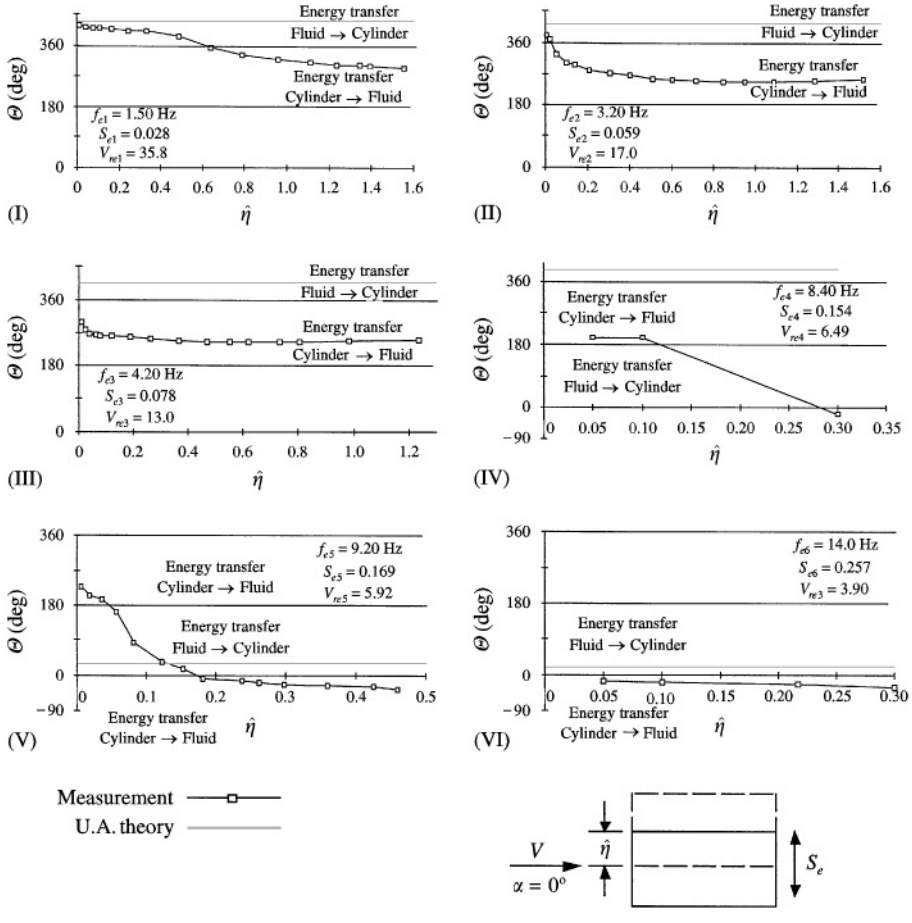

Figure 7(b) Phase angle Θ of the rectangular cylinder for different oscillation frequencies S_e (I–VI) as a function of the dimensionless oscillation amplitude, $\hat{\eta}$, for Re $= 10^5$ and $\alpha = 0°$; comparison of experiment with the unsteady airfoil (UA) theory.

Lift force coefficients $\hat{C}_{Le}$, determined by the unsteady airfoil theory, increase linearly with the amplitude of oscillation and agree well with the experimental data for the lowest ($S_{e1} = 0{\cdot}028$, in the galloping range) and highest ($S_{e6} = 0{\cdot}257$, in the added mass range) frequencies investigated in Figure 7(a). For the other excitation frequencies, the unsteady airfoil theory is capable of predicting only trends of the experimentally measured curves. For the excitation frequencies near the frequency of Kármán vortex shedding ($S_{e2} = 0{\cdot}059$ and $S_{e3} = 0{\cdot}078$), the magnitudes of the lift forces are underestimated, whereas these forces are slightly overestimated for the excitation frequencies near the frequency of impinging vortices ($S_{e4} = 0{\cdot}154$ and $S_{e5} = 0{\cdot}169$). For the excitation frequencies near the frequency of Kármán vortex shedding [Figure 7(a), II and III], the experimentally determined lift forces increase rapidly below $\hat{\eta} \approx 0{\cdot}5$ and are nonlinear for small amplitudes. Above this oscillation amplitude ($\hat{\eta} \approx 0{\cdot}5$) the lift forces increase linearly.

Since the quasi-steady theory is a model for predicting low frequency galloping oscillations, it is only applicable to the lowest excitation frequency, $S_{e1} = 0{\cdot}028$ investigated. However, even at this lowest frequency, the quasi-steady theory loses its validity with increasing amplitude of oscillation above $\hat{\eta} > 0{\cdot}6$ [Figure 7(aI)].

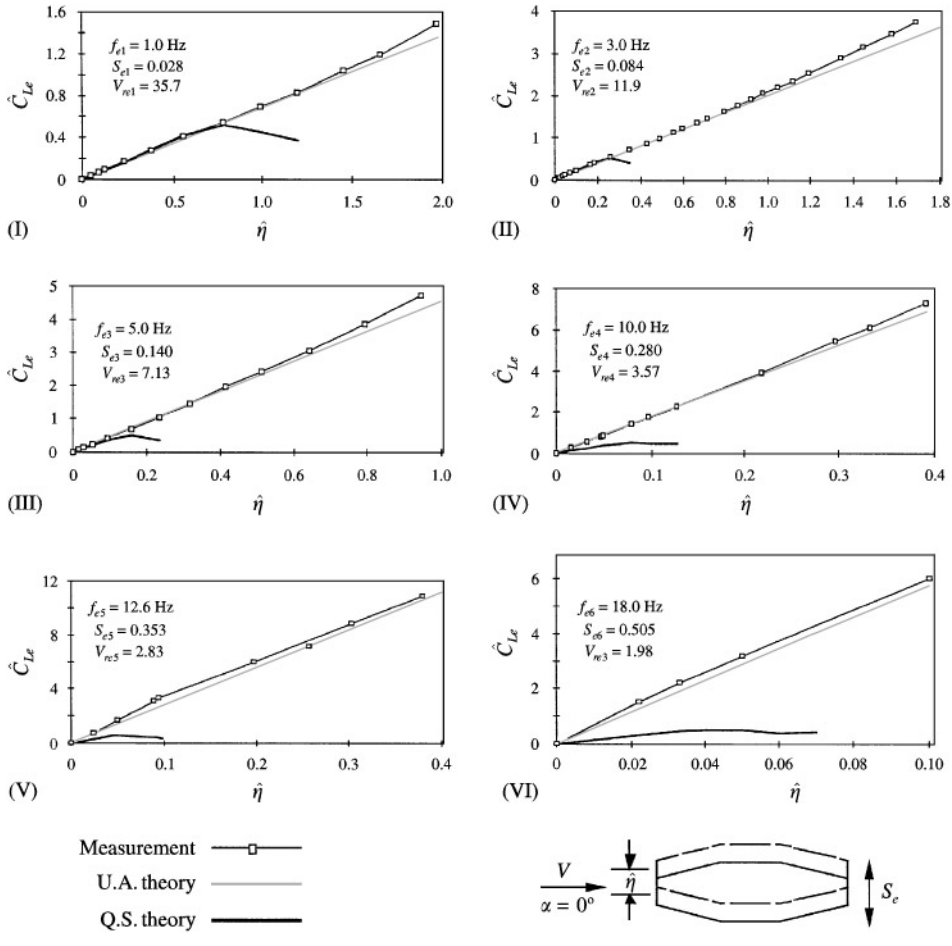

Figure 8(a) Lift coefficient $\hat{C}_{Le}$ of the octagonal cylinder for different oscillation frequencies S_e (I–VI) as a function of oscillation amplitude, $\hat{\eta}$ for $\mathrm{Re} = 10^5$ and $\alpha = 0°$; comparison of experiment with the quasi-steady (QS) theory and the unsteady airfoil (UA) theory.

The phase angle curves of the rectangular cylinder for $\alpha = 0°$ are depicted in Figure 7(b). Both for the frequencies near the frequency of Kármán vortex shedding ($S_{e2} = 0{\cdot}059$ and $S_{e3} = 0{\cdot}078$) and the highest frequency ($S_{e6} = 0{\cdot}257$), the phase angle is almost constant (except for very small oscillation amplitudes), and the energy transfer is from the cylinder to the fluid. For the lowest excitation frequency, $S_{e1} = 0{\cdot}028$ [Figure 7(bI)], which is in the galloping range, a phase angle $\Theta > 360°$ is observed for low oscillation amplitudes. Therefore, the energy transfer is from the fluid to the cylinder, explaining the galloping excitation of the rectangular cylinder for $\alpha = 0°$.

When a cylinder oscillates in a direction transverse to the free stream, its angle of attack α varies continuously; therefore the magnitude of $\hat{\alpha}$ is related to $\hat{\eta}$ and S_e, as defined in $\hat{\alpha} = \tan^{-1}[\hat{\dot{y}}/V] = \tan^{-1}[2\pi\hat{\eta}S_e]$. For $\hat{\eta} \approx 0{\cdot}6$ at $S_{e1} = 0{\cdot}028$ [Figure 7(bI)], where the energy transfer changes sign, a magnitude of $\hat{\alpha} = 6°$ is calculated. This corresponds to the value of α where the stationary C_y versus α curve [Figure 1(a)] also changes its sign. For $\alpha < 6°$, galloping excitation is to be expected, because $\partial C_y/\partial\alpha$ is negative. From $\alpha > 6°$, $\partial C_y/\partial\alpha$ is positive, and that means (according to Den Hartog's instability criteria) no galloping excitation occurs in this range. Since the energy transfer is from the cylinder to the

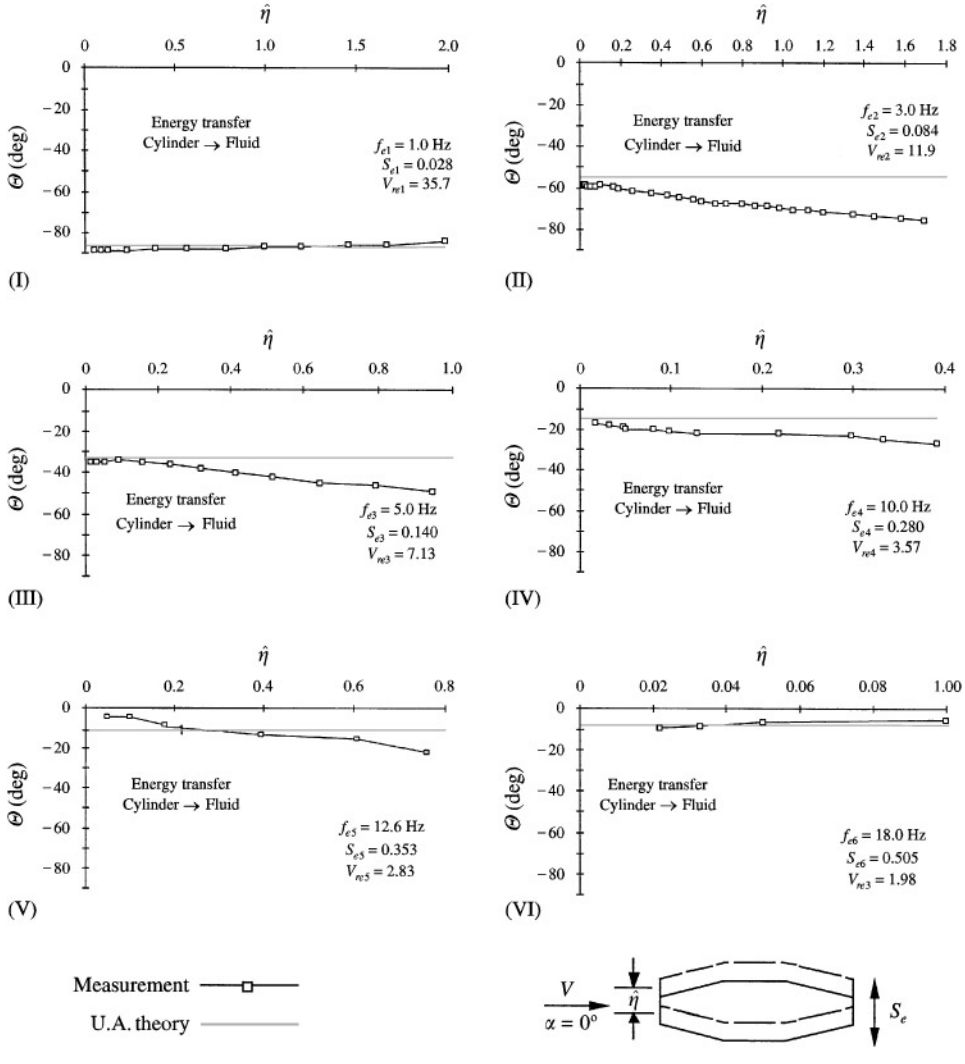

Figure 8(b) Phase angle Θ of the octagonal cylinder for different oscillation frequencies, S_e (I–VI) as a function of oscillation amplitude $\hat{\eta}$, for Re = 10^5 and $\alpha = 0°$; comparison of experiment with the unsteady airfoil (UA) theory.

fluid for $\hat{\eta} > 0{\cdot}6$ [in Figure 7(bI)], the phase angle curve confirms Den Hartog's instability criterion at the excitation frequency $S_{e1} = 0{\cdot}028$ for the rectangular cylinder.

Phase angle curves for the excitation frequencies near the frequency of impinging vortices, S^*, ($S_{e4} = 0{\cdot}154$ and $S_{e5} = 0{\cdot}169$) show similar behavior. For these frequencies, a strong dependence on the oscillation amplitude, $\hat{\eta}$, and a change in the sign of the energy transfer as a function of the oscillation amplitude both occur together.

Above a certain value of the oscillation amplitude, the phase angle remains constant for almost all frequencies investigated in Figure 7(b), implying a limited influence of the oscillation amplitude. In addition, the flow-induced oscillations at a particular oscillation frequency are also limited because, above a certain oscillation amplitude level, the phase angle always shows an energy transfer from the cylinder to the fluid. Prediction of the phase angle by the unsteady airfoil theory does not take the influence of the oscillation amplitude into consideration [see equation (26)] and therefore provides constant values of phase

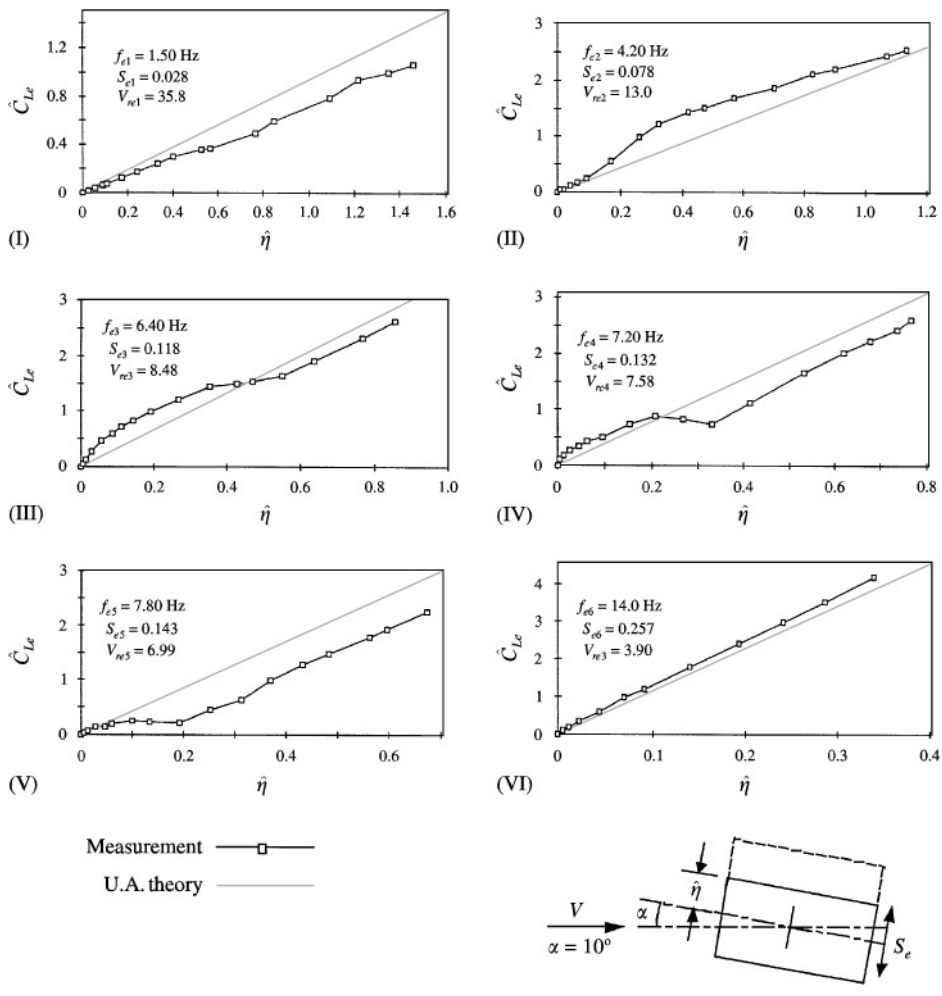

Figure 9(a) Lift coefficient $\hat{C}_{Le}$ of the rectangular cylinder for different oscillation frequencies, S_e (I–VI) as a function of oscillation amplitude, $\hat{\eta}$ for Re $= 10^5$ and $\alpha = 10°$; comparison of experiment with the unsteady airfoil (UA) theory.

angle. The unsteady airfoil theory gives phase angles $0 < \Theta < \pi$ (or $2\pi < \Theta < 3\pi$) for the rectangular cylinder, because $\partial C_L/\partial\alpha$ is negative for $\alpha = 0°$. Thus, the predicted phase angle ranges always show an energy transfer from the fluid to the cylinder, which agrees with the experimental data only for the lowest excitation frequency, $S_{e1} = 0{\cdot}028$, in the galloping range and up to $\hat{\eta} = 0{\cdot}5$. For the other cases investigated, the unsteady airfoil theory is not usable for phase angle predictions of the rectangular cylinder for $\alpha = 0°$.

On the other hand, for the octagonal cylinder at $\alpha = 0°$, where no galloping excitation occurs and the influence of vortex-induced phenomena is small, the predictions of both lift force C_{Le} and phase angle Θ by the unsteady airfoil theory agree well with the experimental data. The measured C_{Le} values increase linearly with the amplitude of the oscillation [Figure 8(a)] and the measured phase angles remain almost constant for all excitation frequencies investigated. Again, an agreement between predictions by the quasi-steady theory and measurements exists only at the lowest excitation frequency, $S_{e1} = 0{\cdot}028$ [Figures 8(aI) and 8(bI)] both for phase angle ($\Theta = -90°$) and for C_{Le} (up to $\hat{\eta} \approx 0{\cdot}8$).

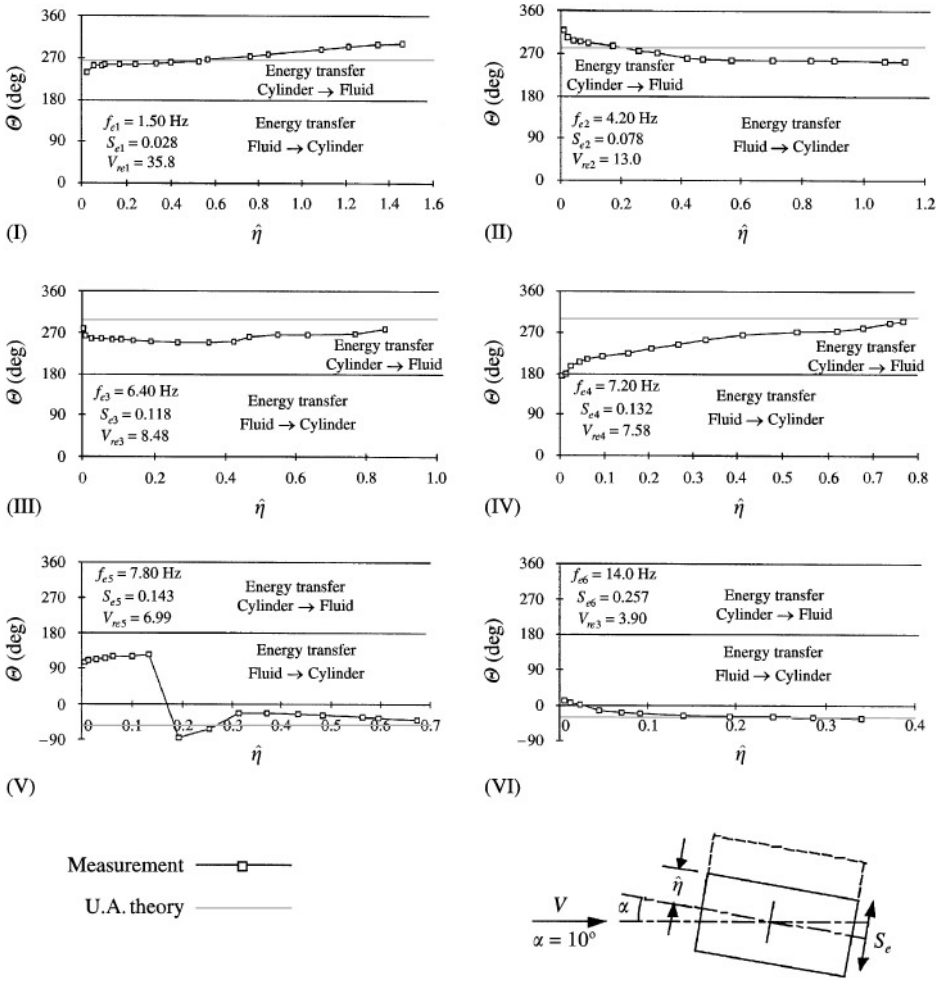

Figure 9(b) Phase angle Θ of the rectangular cylinder for different oscillation frequencies, S_e (I–VI) as a function of oscillation amplitude, $\hat{\eta}$, for Re = 10^5 and $\alpha = 10°$; comparison of experiment with the unsteady airfoil (UA) theory.

For the rectangular cylinder with a mean incidence ($\alpha = 10°$), the lift force coefficients, C_{Le}, and phase angles, Θ, are displayed in Figure 9(a, b) at different excitation frequencies. At the highest frequency investigated, $S_{e6} = 0{\cdot}257$, the lift force coefficient increases linearly with the oscillation amplitude, and the phase angle is nearly constant. Predictions of both the lift coefficient and phase angle by the unsteady airfoil theory agree well with the experimental data for this frequency. The same observation is valid for the lowest excitation frequency, $S_{e1} = 0{\cdot}028$, except that the unsteady airfoil theory underestimates the experimental lift coefficient. The frequencies in between ($S_{e3} = 0{\cdot}118$, $S_{e4} = 0{\cdot}132$, $S_{e5} = 0{\cdot}143$, and partly $S_{e2} = 0{\cdot}078$) show similar trends of the experimentally determined lift coefficients as a function of the oscillation amplitude [Figures 9(aII)–(9aV)]. An increase in the lift coefficient for small oscillation amplitudes halts, corresponding to a range in oscillation amplitude where the lift coefficients do not increase with increasing oscillation amplitude. At the end of this range, lift coefficients continue increasing linearly with the oscillation amplitude and are parallel to the predicted curves determined by the unsteady airfoil theory. The turning point of the lift curve, which depends upon the excitation frequency,

shifts to smaller oscillation amplitudes with increasing excitation frequency. For $S_{e5} = 0{\cdot}143$ [Figure 9(aV)] there is almost no increase in the lift coefficient at low oscillation amplitudes. This excitation frequency of $S_{e5} = 0{\cdot}143$ corresponds to a frequency range where the lift coefficient develops a local minimum after a maximum due to a resonance at the Kármán vortex frequency [see Figure 5(a)]. It is also in the frequency range of the phase jump [see Figure 6(a)].

Similar minima for the lift coefficient in the range of phase jump were also observed by Staubli & Rockwell (1989) for an oscillating trailing-edge and by Bearman & Luo (1988) for the square-section cylinder. This lift minimum is caused by the reattachment of the flow on one side of the square cylinder at this value of the angle of attack. Bearman & Luo (1988) calculated the value for the angle of attack, $\hat{\alpha}$, in the range of minimum lift force coefficient and compared it with the curve of the stationary lift force versus angle of attack. Similar calculations of the value for angle of attack, $\hat{\alpha}$, for the rectangular cylinder do not show any correlation between the minimum of the lift force and stationary lift force versus angle of attack curve. The regions, where the lift coefficient shows large changes, depend on the excitation frequency, as well as on the amplitude of oscillation, as seen in Figure 9(a). For the excitation frequency $S_{e5} = 0{\cdot}143$ [Figure 9(bV)], the phase angle curve exhibits a phase jump as a function of oscillation amplitude. The abrupt change in the phase angle means a change of the vortex formation in the near wake of the cylinder. Therefore, the large changes in the lift coefficient in Figure 9(a) [and also Figure 5(a)] should be caused by the formation of vortical structures at the leading- and trailing edge of the rectangular cylinder. For a better understanding of this observed phenomenon in the case of the rectangular cylinder for $\alpha = 10^\circ$, visualization of the flow field is necessary. In a similar frequency range, namely after the synchronization region with Kármán vortex shedding, flow visualization for the rectangular cylinder for $\alpha = 0^\circ$ (Deniz & Staubli 1997) showed that major changes occur in the wake with respect to the alternating vortex formation, causing the annihilation of induced lift forces and local minima of lift coefficients.

5. REMARKS AND CONCLUSIONS

Parkinson's quasi-steady theory predicts lift forces and flow-induced oscillations well for low oscillation frequencies, as demonstrated by several authors through comparisons of predictions with experimental results for cylinders of various shapes (especially for the square-section cylinder). In the present investigation, the quasi-steady theory is used to predict the lift forces for transversally oscillating rectangular and octagonal cylinders. The limit of the quasi-steady theory is found at nondimensional oscillation frequencies of $S_e < 0{\cdot}04$ for the rectangular cylinder and $S_e < 0{\cdot}12$ for the octagonal cylinder. The quasi-steady theory has also limitations to its validity in the low-frequency range with regard to the maximum amplitude of oscillation, $\hat{\eta}$.

The unsteady airfoil theory, which had been originally developed for the small amplitude oscillations of airfoils and thin plates, was employed by Luo & Bearman (1990) for a square-section cylinder. The agreement with the experiments reflects that the Theodorsen function and lift curve slope values in the unsteady airfoil approach (that have been obtained from stationary cylinders) can be used in predictions of the quasi-steady fluid forces for low-frequency oscillations and of the inertia effects at high-frequency oscillations.

Besides inertia effects, an oscillating cylinder sheds motion-induced vortices. Such vortex formation depends largely on the shape of the oscillating cylinder, i.e. reattachment may occur. Obviously, predictions by the unsteady airfoil theory are better for slender profiles, as confirmed by the two cylinders investigated, of which the octagonal one gives better agreement.

The quasi-steady theory assumes that the phase angle, Θ, between the lift force and the cylinder displacement at the excitation frequency has a constant value of $\pm \pi/2$, depending upon the slope of the lift characteristic. Experimental results confirm this value of the phase angle for very low oscillation frequencies. The unsteady airfoil theory includes phase information about the resulting lift force, thereby giving quantitative information on the energy transfer from the fluid to the cylinder. For the cases with positive energy transfer from the fluid to the cylinder, self-excited cylinder oscillations are possible. The existence of such a region for the rectangular cylinder both at $\alpha = 0^\circ$ and low oscillation frequencies, indicates galloping excitation, and the unsteady airfoil theory is able to predict this case. Another case, where the unsteady airfoil theory estimates the experimental trend of phase angle and the energy transfer well, is the rectangular cylinder oscillating with a mean incidence of $\alpha = 10^\circ$, with the exception of the region of the phase jump.

For the octagonal cylinder investigated, where galloping instability is not observed and the influence of instability-induced phenomena (such as vortex shedding) is small, the predictions of the lift force as well as phase angle by unsteady airfoil theory agree well with the experimental results in a broad range of oscillation frequency. In the case of oscillations at a mean incidence of $\alpha = 10^\circ$, the phase prediction is wrong in sign; this can be explained by the fact that Den Hartog's instability criterion fails for the octagonal cylinder at this mean incidence.

For the rectangular cylinder at intermediate values of oscillation frequency, S_e, instability-induced effects such as Kármán vortex-shedding and/or impinging vortices dominate the flow field for oscillations without ($\alpha = 0^\circ$) as well as with a mean incidence ($\alpha = 10^\circ$). Predictions are incorrect by either theory within these instability-influenced ranges. Recently, Scanlan *et al.* (1996) have also demonstrated the failure of the Theodorsen circulation function and the unsteady airfoil theory to account for the oscillatory lift of rectangular profiles.

The investigation of linearity with increasing amplitude of oscillation, $\hat{\eta}$, was carried out in the second part of this study for both the rectangular and octagonal cylinders at $\alpha = 0^\circ$ and $\alpha = 10^\circ$. In these experiments the amplitude of oscillation exerts a nonlinear influence mainly in the frequency ranges of instability-induced phenomena. Therefore, for the octagonal cylinder, linearity with the oscillation amplitude is found both in cases without and with mean incidence.

On the other hand, the measured lift force and phase angle curves of the rectangular cylinder show significant nonlinear dependence on the oscillation amplitude in the frequency range of instability-induced phenomena, for both cases without ($\alpha = 0^\circ$) and with ($\alpha = 10^\circ$) a mean incidence. However, the nonlinear influence of the oscillation amplitude is limited to a certain maximum value. Above this limit oscillation amplitude, the lift forces increase linearly, while the phase angle remains nearly constant. The important fact is that for a constant excitation frequency the sign of the phase angle and therefore the direction of energy transfer can change with oscillation amplitude.

One important design criterion for the octagonal cylinder is that it is less susceptible to flow-induced oscillations. The lift-curve slope at $\alpha = 0^\circ$ is positive and no galloping oscillations occur. In the overall oscillation frequency and amplitude ranges investigated, the phase angle indicates energy transfer from the cylinder to the fluid. The amplification of the fluctuating lift force due to Kármán vortex shedding in the wake is also very small. For the case without incidence ($\alpha = 0^\circ$), the flow separates at the leading edges, but reattaches within a very short distance, remains attached to the side surfaces, and finally separates at the trailing edges. Since the profile thickness at the trailing edge is smaller than the profile thickness, D, the wake and the width of the Kármán vortex street are narrow. Another reason for the small lift amplification due to Kármán vortex shedding is that sharp leading edges decrease the periodicity of the vortex shedding. Due to sharp leading and trailing

edges, the flow characteristics of the octagonal cylinder are also Reynolds-number-independent.

References

Bearman, P. W. & Luo, S. C. 1988 Investigation of the aerodynamic instability of a square-section cylinder by forced oscillation. *Journal of Fluids and Structures* **2,** 161–174.

Bearman, P. W., Gartshore, I. S., Maull, D. J. & Parkinson, G. V. 1987 Experiments on flow-induced vibration of a square-section cylinder. *Journal of Fluids and Structures* **1**, 19–34.

Bisplinghoff, R. L., Ashley, H. & Halfman, R. L. 1957 *Aeroelasticity*. Cambridge, MA: Addison-Wesley.

Brar, P. S., Raul, R. & Scanlan, R. H. 1996 Numerical calculation of flutter derivatives via indicial functions. *Journal of Fluids and Structures* **10,** 337–351.

Blevins, R. D. 1990 *Flow-Induced Vibrations*. New York: Van Nostrand Reinhold.

Den Hartog, J. P. 1956 The vibration problems of engineering. In *Proceedings 4th International Congress of Applied Mechanics*, Cambridge, pp. 34–53.

Deniz, S. & Staubli, T. 1997 Oscillating rectangular and octagonal profiles: Interaction of leading- and trailing-edge vortex formation. *Journal of Fluids and Structures* **11,** 3–31

Deniz, S. 1993 Kräfte auf angeströmte, schwingende Profile mit Rechteck- und Achteckquerschnitt. Dissertation No 10341, Swiss Federal Institute of Technology, Zürich, Switzerland.

Dowell, E. H., Curtiss, H. C., Scanlan R. H. & Sisto, F. 1989 *A Modern Course in Aeroelasticity*. 2nd edition. Dordrecht: Kluwer Academic Publishers.

Försching, H. 1974 *Grundlagen der Aeroelastik*. Berlin: Springer Verlag.

Franke, R. 1991 Numerische Berechnung der instationären Wirbelablösung hinter zylinderischen Körpern. Ph.D. Dissertation, University of Karlsruhe, Karlsruhe, Germany.

Griffin, O. M. & Ramberg, S. E. 1974 The vortex-street wakes of vibrating cylinders. *Journal of Fluid Mechanics* **66,** 553–576.

Groh, G. 1992 Computation of hydrodynamic mass for general configurations. In *Proceedings ASME Symposium on Flow Induced Vibrations*, Anaheim, CA, U.S.A.

Hartlen, R. T. & Currie, I. G. 1970 Lift-oscillator model of vortex-induced vibration. *ASCE Journal of the Engineering Mechanics Division* **96,** 577–593.

Karman, von T. & Sears, W. R. 1938 Airfoil theory for non-uniform motion. *Journal of Aeronautical Sciences* **5,** 379–390.

Luo, S. C. & Bearman, P. W. 1990 Predictions of fluctuating lift on a transversely oscillating square-section cylinder. *Journal of Fluids and Structures* **4,** 219–228.

Matsumoto, M., Kobayashi, Y., Nihara, Y., Shirato, H. & Hamasaki, H. 1995 Flutter mechanism and its stabilization of bluff bodies. In Proceedings of the Ninth Conference on Wind Engineering, Vol. II, pp. 827–838, New Delhi, India.

Matsumoto, M. 1971 The dynamical forces acting on the vibrating square prism in a steady flow. In *International Conference on Wind Effects on Buildings and Structures*, pp. 921–930, Tokyo, Japan.

Nakamura, Y. & Mizota, T. 1975 Unsteady lifts and wakes of oscillating rectangular prisms. ASCE *Journal of the Engineering Mechanics Division.* **101,** 855–871.

Naudascher, E. & Rockwell, D. 1994 *Flow-Induced Vibration—An Engineering Guide*. Rotterdam: Balkema.

Novak, M. N. 1972 Galloping oscillations of prismatic structures. ASCE *Journal of the Engineering Mechanics Division* **98,** 27–41.

Parkinson, G. V. 1989 Phenomena and modeling of flow-induced vibrations of bluff bodies. *Progress in Aerospace Science* **26,** 169–224.

Parkinson, G. V. 1971 Wind-induced instability of structures. *Philosophical Transactions of the Royal Society, London Series A*, **269,** 395–409.

Parkinson, G. V. & Smith, J. D. 1964 The square prism as an aeroelastic non-linear oscillator. *Quarterly Journal of Mechanics and Applied Mathematics* **17,** 225–239.

Parkinson, G. V. & Brooks, N. P. H. 1961 On the aeroelastic instability of bluff cylinders. *Journal of Applied Mechanics* **28,** 225–258.

Sarpkaya, T. 1989 Computational methods with vortices—The Freeman scholar lecture. *ASME Journal of Fluids Engineering* **111,** 5–52.

Scanlan, R. H., Jones, N. P. & Singh, L. 1996 Interrelations among flutter derivatives. *Proceedings Colloquium on Bluff-Body Aerodynamics and Applications II*, Virginia Tech, Blacksburg, VA, U.S.A.

Scanlan, R. H., Beliveau, J. G. & Budlong, K. S. 1974 Indicial aerodynamic functions for bridge decks. *ASCE Journal of the Engineering Mechanics Division* **100,** 657–672

Scanlan, R. H. & Tomko, J. J. 1971 Airfoil and bridge deck flutter derivatives. *ASCE Journal of the Engineering Mechanics Division* **97,** 1717–1737

Staubli, T. & Rockwell, D. 1989 Pressure fluctuations on an oscillating trailing edge. *Journal of Fluid Mechanics* **203,** 307–346,

Staubli, T. 1983 Untersuchung der oszillierenden Kräfte am querangeströmten, schwingenden Kreiszylinder. Dissertation No 7322, Swiss Federal Institute of Technology, Zürich, Switzerland.

Tamura, T. & Kuwahara, K. 1992 Numerical study on aerodynamic instability of oscillating rectangular cylinders. *Journal of Wind Engineering and Industrial Aerodynamics* **41,** 253–254

Theodorsen, T. A. 1935 General theory of aerodynamic instability and mechanism of flutter. NACA Technical Report No. 496, pp. 413–433.

Williamson, C. H. K. & Roshko, A. 1988 Vortex formation in the wake of an oscillating cylinder. *Journal of Fluids and Structures* **2,** 355–369.

APPENDIX: NOMENCLATURE

A	area of cylinder (length × span)
A'	fluid dynamic mass
B	structural damping
B'	fluid dynamic damping
C	structural rigidity
C'	fluid dynamic rigidity
C_D	drag coefficient
C_L	lift coefficient
C_y	transverse fluid force coefficient
$C(k)$	Theodorsen function, $C(k) = F(k) + \mathrm{i}G(k)$
D	thickness of cylinder
f_e	excitation frequency (Hz)
F_L	lift force
F_{Lad}	lift force due to the fluid inertia or added mass
$F(k)$	real part of Theodorsen function
$G(k)$	imaginary part of Theodorsen function
$\mathrm{H}_0^{(2)}$	Hankel function of second kind of order 0
$\mathrm{H}_1^{(2)}$	Hankel function of second kind of order 1
k	reduced frequency, $k = \omega D/V$
L	length of cylinder
m	mass of cylinder
Re	Reynolds number, $\mathrm{Re} = VL/v$
S	Strouhal number, $S = fD/V$
S_e	nondimensional excitation frequency, $S_e = f_eD/V$
S^*	nondimensional frequency of impinging vortices, $S^* = f^*D/V$
S_{o}	nondimensional frequency of wake vortex formation, $S_{\mathrm{o}} = f_{\mathrm{o}}D/V$
t	time
V	free-stream velocity
V_{rel}	relative velocity
V_{re}	reduced velocity, $V_{\mathrm{re}} = V/f_eD$
y	displacement of cylinder
$\dot{y}$	velocity of cylinder oscillation
$\ddot{y}$	acceleration of cylinder oscillation
α	angle of attack
$\hat{\eta}$	nondimensional amplitude of oscillation, $\hat{\eta} = \hat{y}/D$
Θ	phase angle between cylinder displacement and lift force
λ	nondimensional flow inertia coefficient
v	kinematic viscosity
ρ	density of fluid
ω	angular frequency (rad/s)
$\hat{}$	magnitude